AMS Home   Journals Home   Journal Archive   Subscribe   For Authors   Help   Advanced Search   [Search] [Go]

Full Text View

Wind-Driven, Coastal-Trapped Waves off the Island of Gotland, Baltic Sea

Oscar Pizarro

Department of Oceanography, Earth Sciences Centre, University of Göteborg, Goteborg, Sweden, and School of Marine Sciences, Catholic University of Valparaiso, Valparaiso, Chile

Gary Shaffer

Danish Center for Earth System Science, Niels Bohr Institute for Astronomy, Physics and Geophysics, University of Copenhagen, Copenhagen, Denmark

ABSTRACT

An analysis is presented of repeated density and current profiles and recording current meter (RCM) data collected off the northwest coast of Gotland Island (Baltic Sea) during the late summer and fall of 1977. Large, low-frequency fluctuations were found in alongshore flow and isopycnal displacements and were significantly correlated with winds observed at Gotland's west coast. The best correlations were found with winds from the island's southern tip rather than with local winds. Coherence was high between RCM current fluctuations at 70 and at 90 m (100 m water depth, 4 km from the coast), whereby flow at 90 m led flow at 70 m. An EOF analysis of profile observations showed a 7-day, baroclinic wave with a two- and a three-layer current structure "trapped" in the coastal zone. The time series of the (weaker) three-layer mode was found to lag that of the (stronger) two-layer mode by about one day.

Wind-forced, coastal-trapped wave (CTW) theory (with bottom friction and scattering) was applied to the Gotland west coast and model output was compared with data. This application assumed zero CTW amplitude at the island's southern tip, the starting point for the forced-wave integration, and used two coastal segments, a late summer and a winter stratification, and winds from three coastal sites. A very simple model version (first two CTW modes only, no bottom friction or scattering, winds from the island's southern tip only) was able to reproduce reasonably well structure, amplitudes, and phases of observed alongshore current fluctuations in the lower part of the water column. Observed upward phase propagation was explained by lagged superposition of the two CTW modes. In the strongly stratified Baltic Sea, buoyancy forces may act to reduce the effects of bottom friction on low-

Options:
- Create Reference
- Email this Article
- Add to MyArchive
- Search AMS Glossary

Search CrossRef for:
- Articles Citing This Article

Search Google Scholar for:
- Oscar Pizarro
- Gary Shaffer

frequency flow. A combination of island length scale and synoptic wind scales act to "filter out" higher CTW modes. The effects of scattering were greatest for weaker, winter stratification.

1. Introduction

Observations in large lakes and semienclosed seas reveal strong, low-frequency variability of currents and stratification near coasts (cf. Csanady 1981). In midlatitudes, this variability is strongly coupled to synoptic-scale winds. Linear, quasigeostrophic theory has proven useful in interpreting these observations since this theory predicts the existence of free, low-frequency wave modes trapped near a coast (cf. Brink 1991). These coastal-trapped waves can be represented by a sum of modes whose structures and phase velocities depend on cross-shore topography and stratification. The amplitude of each mode depends on the wind forcing experienced during its journey and on the dissipation by friction and scattering of energy to other modes or other kinds of motion. As the perturbations in the coastal zone increase in size, nonlinear and frictional effects become more important. Coastal jets, upwelling, and large pycnocline displacements in the coastal zone favor strong vertical exchange there. Such enhanced exchange in a relatively narrow zone near the coast may dominate the total vertical exchange within a given basin (Shaffer 1979).

The Baltic Sea has been the site of pioneering research in oceanography. For instance, some of the first observations of inertial oscillations were reported there (Gustafsson and Kullenburg 1933). However, there have been few studies on the dynamics of the coastal zone in the Baltic Sea. In the first such study, Walin (1972a,b) considered the generation of Kelvin waves by the wind and their role in the strongly stratified Baltic Sea. Walin used temperature observations from a section off the southeast coast of Sweden and local wind data to identify wind-forced, baroclinic disturbances, trapped near the coast and traveling south along it like first baroclinic mode Kelvin waves. Lass and Talpsepp (1993) observed coastal-trapped current oscillations off the northern coast of Germany and interpreted these as (barotropic) continental shelf waves.

About 20 years ago, one of us (GS) led a series of field studies in the northwest Baltic Proper between the large island of Gotland ($\sim$ 150 km long, $\sim$ 40 km wide) and the Swedish mainland south of Stockholm (Fig. 1 ⊙). In one such study in 1976, a current profiling section between the mainland and Gotland revealed strong, baroclinic flow within an internal radius of deformation (about 5 km) of the northwest coast of Gotland (Shaffer 1979). Such structure strongly suggests internal Kelvin-wave-like dynamics in this region with a steep coastal boundary and nearly flat bottom topography. These results motivated an intensive field study in the same Gotland coastal zone during the late summer and fall of 1977. This latter study, which combined high spatial and high temporal resolution views of the region, was carried out with success but results from it have not been reported previously. Here we present an analysis of the 1977 data whereby we draw upon recent theoretical advances on forcing, dissipation, frictional coupling, and scattering of general coastal-trapped waves.

2. Study area, experiment, and data reduction

The Baltic Sea is a large estuary with a permanent salinity stratification, characterized in the Baltic Proper (Fig. 1 ⊙) by a strong halocline at a depth of 60–70 m. In the Baltic Proper, a seasonal thermocline develops at about 20-m depth in the summer, deepens during the fall, and disappears by early winter. Our field observations were concentrated in a small area off the northwest coast of Gotland about 15 km north of Visby and about 100 km north of Hoburg at the southern tip of the island (Fig. 1 ⊙). Bottom topography along the west coast of Gotland is characterized by a rather broad shelf (more than 20 km wide) in the southern third and a narrow shelf (about 5 km wide) in the northern half, separated by a transition zone. The water depth seaward of the shelf is about 105 m. Relatively shallow "ridges" extend to the north and to the south from the island.

Between 23 August and 1 September 1977 profiling sections were run each day in the study area (Fig. 1 ⊙). Each of the ten sections consisted of six stations, extended 17 km from the coast, and took about 2.5 h to complete. The following data were collected at each station: 1) continuous vertical conductivity, temperature, and depth (CTD) profiles from the surface to the bottom, and 2) profiles of absolute currents from lines of individual currents measurements with 5-m vertical separation from about 5 m over the bottom to about 10–15-m depth. Each daily section contained about 90 individual current observations. In addition, hydrographic casts were made at some stations for CTD calibration. Currents were measured with gelatin pendulum current meters (PCM; Haamer 1974) with an accuracy of about 2 cm s^{-1} in speed and about 5° in direction [Cederlöf et al. (1996) report results of a field intercalibration of PCMs with three standard types of recording current meters]. Since the PCMs were attached at fixed intervals from the bottom up, different station depths for repeated profiles at a given station lead to different PCM depths. To facilitate comparison of data from individual days, PCM (and CTD) data were interpolated to fixed depths at 5-m intervals using semi-Hermite splines (Akima 1970). A total of 86 fixed depths were thus defined across the section.

Three Aanderaa RCM-4 recording current meters (RCM) were deployed on a taut wire mooring at station 3 (Fig. 1 ⊙) on 17 August 1977 and recovered on 21 November 1977. Estimated depths for the RCMs were 50, 70, and 90 m (water

depth of about 100 m). Each RCM recorded current speed and direction with a 15-min sampling period. Good data were collected only at 70 and 90 m. Wind data every 6 h were obtained at Hoburg, Stora Karlsö, and Visby (Fig. 1 ⊙) from the Swedish Meteorological and Hydrological Institute. These positions are located about 100 km, 60 km, and 15 km south of the study area. Wind stress was calculated from these observations using a constant drag coefficient of 1.3×10^{-3} and air density of 1.2 kg m^{-3}. Hourly, vector-averaged RCM current data and wind data interpolated to one hour were low-pass (LP) filtered with a 121-point cosine Lanczos filter with half power at 40 h. Subsequently, all time series were resampled every 6 hours.

3. Time series results

Means, variances, covariances, and eddy kinetic energy of LP currents at 70 and 90 m for the period 20 August to 18 November are shown in Table 1 ⊙. Cross-shore and alongshore current components, u and v, are taken to be positive toward 113° and 23°, respectively. This orientation is based on principal axes calculated from the LP current records and agrees well with the local coastal orientation. Mean alongshore flow of 5.0 and 3.8 cm s^{-1} was observed at 70 and 90 m, respectively, during the period. The observed cross-shore flow is seaward at 90 m, as would be expected in a bottom Ekman layer given the observed alongshore flow. Current fluctuations were slightly stronger at 70 m than at 90 m. Spectra of the raw currents (not shown) confirmed that energy in the low-frequency band (periods ≥100 h) dominated at both depths.

The low-passed alongshore wind stress at Hoburg, Stora Karlsö, and Visby were quite similar, dominated by synoptic-scale (3–10 day) events (Fig. 2 ⊙). The low-passed time series of alongshore flow at 70 and 90 m show synoptic-scale fluctuations with velocities up to 50 cm s^{-1} (Fig. 2 ⊙). Alongshore flow at 70 m was strongly correlated with and lagged that at 90 m (maximum correlation of 0.79 at 6-h lag, significant to 99%). Positive events in alongshore current occurred in consort with negative wind stress events. The alongshore current at 70 m (90 m) was significantly correlated with the Visby alongshore wind stress with maximum values of −0.62 (−0.59) at 18 (12) h lag (positive current lags negative wind stress). Maximum correlation and lag at 70 m (90 m) increased somewhat to −0.66 (−0.62) and 18 (12) h with the Stora Karlsö wind stress and to −0.68 (−0.69) and 24 (18) h with the Hoburg wind stress.

High coherence between alongshore flow at 70 and 90 m at station 3 and Visby alongshore wind stress was found in the synoptic band centered at about 4.5 days (Fig. 3a ⊙). The band of high coherence between observed currents and Hoburg wind stress (Fig. 3b ⊙) is much broader, including fluctuations of up to several weeks. Other studies have also shown greater coherence at low frequencies between observed alongshore flow and alongshore wind stress upstream (in the coastal-trapped wave sense) from the observation site than between such flow and local wind stress (cf. Denbo and Allen 1987). Alternatively, the winds observed at Hoburg may be more representative for winds off Gotland since the Visby observation site may be less exposed. Phase results between alongshore wind stress and alongshore flow show values near 180° at very low frequencies and a rather linear decrease in phase toward higher frequencies (Figs. 3c,d ⊙). These results imply that negative wind stresses at Visby and Hoburg lead positive alongshore flow in the deep layers at station 3 by 12–24 h over a quite broad frequency range. At least two factors might help to explain this result. First, the spin-up time of wind-driven flow is related to the inertial period, 14.2 h in the study region. Second, first-mode coastal-trapped waves are nondispersive at low frequencies (cf. Brink 1991); thus such waves of different frequencies would take about the same time to traverse the west coast of Gotland. The time and space scales involved (about 100 km, about 1 day) lead to a rough propagation speed estimate of about 1 m s^{-1}.

The coherence between alongshore flow observed at 70 and 90 m was high for fluctuations with periods of 3 days or more (Fig. 3a ⊙). For periods of about a week or more, flow at 90 m clearly led flow at 70 m (Fig. 3c ⊙). For such periods, the above analysis suggested forcing by "remote" winds (coherence of the alongshore flow greater with Hoburg than with Visby wind stress). For periods of about 3–5 days, flow at both depths is essentially in phase (Fig. 3c ⊙) and is most related to local winds (Fig. 3a ⊙).

4. Intensive study results

The intensive study from 23 August to 1 September captured a synoptic-scale fluctuation of moderate amplitude in alongshore wind stress and alongshore flow (between vertical dashed lines in Fig. 2 ⊙). Here we use CTD and PCM data from the ten consecutive profiling sections during this period to examine the time–space structure of this fluctuation. At each station, depths to density surfaces were determined from CTD observations. Means of these depths over the period and deviations from the means (i.e., vertical isopycnal displacements) were then formed (this procedure is superior to time averaging of density at fixed positions since it retains real gradients). Results for the mean cross-shore distribution of isopycnal depth (not shown) reflect summer conditions with the seasonal thermocline depth near 20 m and the permanent halocline depth at 60–70 m. Mean alongshore flow in the period (calculated in usual x–z space, not shown) was generally positive but weak ($\lesssim 5$ cm s^{-1}).

We applied an empirical orthogonal function (EOF) analysis (cf. Davis 1976) to deviations from the mean for alongshore flow and isopycnal depth. EOF analysis provides an efficient means of separating organized motion from "noise." Our particular application is based on 86 points in space (69 points for vertical isopycnal displacement), each with a 10-point time series. Figures 4a and 4b ◉ show the spatial structure of EOF modes 1 and 2 for alongshore velocity (V1 and V2), Fig. 4c ◉ shows EOF mode 1 for vertical isopycnal displacement (D1), and Fig. 4d ◉ shows the time series for each of these modes. Convergence was very rapid: modes V1 and V2 (of a total of 86 modes) accounted for 53% and 22% of total observed variance, respectively, and mode D1 (of a total of 69 modes) accounted for 69% of total observed variance.

Mode V1 has a two-layer structure and captures most of the observed variance in the upper 30–40 m. The largest current amplitudes are found in the upper coastal corner. While relatively weak, lower-layer flow in this mode is concentrated within a few kilometers of the coast; the strong upper-layer flow extends about 10 km offshore (compare with a first internal radius of deformation of 5.6 km based on the observed density distribution). Mode V2 has a three-layer structure with maximum flow at intermediate depths at the coast. In the central part of the section (stations 3–5), variability associated with mode V2 is concentrated below the halocline with an offshore scale similar to the upper-layer flow in mode V1. The maximum amplitude in mode D1 is found at about 50-m depth, greatest near the coast. Its offshore scale was about the same as that of the upper-layer flow in mode V1. Higher EOF V and D modes contained little energy and were not directly interpretable.

The time series for mode V1 is dominated by the synoptic-scale oscillation. The time series for mode D1 exhibits the same oscillation with a slight lag. Calculations of geostrophic shear based on the structure and time series of mode D1, given the basic stratification of the study region, approximate well the observed shear associated with the structure and time series of mode V1. The time series of mode V2 roughly reflects the synoptic-scale oscillation but appears to lag mode V1 considerably, in particular during the first part of the intensive period. Taken together, the time series and intensive study analyses presented above strongly suggest that current variability off the northwest coast of Gotland during the late summer and fall of 1997 was dominated by low-frequency, quasigeostrophic, coastal-trapped motions forced by the local wind.

5. Coastal-trapped waves

a. Theory and definitions

Results of the data analysis above encouraged us to apply a wind-forced, coastal-trapped wave (CTW) model to the coastal zone off the west coast of Gotland. Here we summarize very briefly CTW theory to facilitate the discussion below. This theory has a rich history; details can be found in works cited below. For a linear Boussinesq ocean, frequencies much less than inertial frequency f, and alongshore scales much greater that cross-shelf scales the equations of motion near a coast are solved by expanding the perturbation pressure p as

$$p(x, y, z, t) = \sum_n F_n(x, z)\phi_n(y, t), \qquad (1)$$

where x, y, and z are cross-shelf, alongshore, and vertical coordinates; t is time, F_n are the free CTW modal structures; and ϕ_n are the amplitudes. The alongshore velocity υ is given by the geostrophic relation $-(\rho_0 f)^{-1} p_x$, where ρ_0 is the mean density. The F_n are solutions of an eigenvalue problem with appropriate boundary conditions (including $F_n \rightarrow 0, x \rightarrow \infty$) given a buoyancy frequency $N(z)$ and a water depth $h(x)$, increasing monotonically offshore to a constant depth. The eigenvalues c_n of the problem are the free CTW phase speeds. The F_n are normalized in a way that satisfies energy conservation (Brink 1989).

The ϕ_n in Eq. (1) is determined by integration along the coast of a set of coupled, first-order wave equations subject to forcing by the alongshore wind stress $\tau^y(y, t)$:

$$c_n^{-1}\phi_{nt} - \phi_{ny} - \sum_m a_{nm}\phi_m = b_n\tau^y, \qquad (2)$$

where a_{nm} is the frictional coupling to mode m and b_n is the wind coupling coefficient. The a_{nm}, which account for bottom boundary layer dynamics, are calculated using the F_n and F_m at the bottom and coastal boundaries based on a (linear) bottom stress equal to $\rho_0 r(x)\upsilon_B$, where r is a bottom friction coefficient and υ_B is the bottom velocity (Clarke and Brink 1985). The a are directly proportional to r if r is assumed constant. The b_n are related to the F_n at a vertical coastal wall at $x = 0$ (cf. Mitchum and Clarke 1986).

Large alongshore variations in bottom topography can produce energy exchange (scattering) among CTW modes. Along the west coast of Gotland bottom topography changes significantly (Fig. 1 ⊙) and scattering may occur. CTW bottom pressure perturbation is conserved along coastal isobaths if $\omega/f \ll B$ (where ω is the wave frequency and B is the ratio of the internal radius of deformation to the cross-shelf scale equal to NH/fL, where N, H, and L are typical values of buoyancy frequency, offshore depth, and cross-shelf scale, respectively; see Johnson 1991). The range of B off the west coast of Gotland is about 0.2–1 (see below) and the above condition should hold for periods much greater than two days. Then the following stratified connection formula (Johnson 1991) may be used to estimate CTW scattering:

$$q_{nm} = \int_{-H}^{0} F_n^+ F_m^- \, dz, \qquad (3)$$

where q_{nm} is the scattering ratio of the amplitude of scattered mode n to that of incident mode m, $F = F(d(z), z)$ is evaluated before (+) and after (−) the irregularity in shelf topography, and $d(z)$ is the distance of isobath z from the coast.

b. Application to the west coast of Gotland

The relative importance of stratification and bottom topography in coastal-trapped waves can be measured by the stratification parameter B^2 (Brink 1991). For $B^2 \gg 1$ the waves are affected mainly by stratification and approach baroclinic Kelvin waves. For $B^2 \ll 1$, the waves are affected mainly by variable bottom topography and approach (barotropic) continental shelf waves. Off the southwest coast of Gotland, $B^2 \approx 0.05$ and the first-mode CTW will be highly barotropic. In the study region off the northwest coast of Gotland, $B^2 \approx 1.1$ and both stratification and bottom topography are important for the CTW dynamics.

To compute the F_n, a_{nm}, and b_n for the west coast of Gotland, we used an updated version (January 1995) of the Brink and Chapman (1987) numerical model. The program was run using mean cross-shore bottom topography for segment 1 ("wide" shelf, southwest Gotland) and segment 2 ("narrow" shelf, northwest Gotland) with a vertical coastal wall of 15-m depth and with an N^2 profile (Fig. 5 ⊙) based on the intensive period stratification. Results were quite insensitive to a reasonable range of coastal wall depths (5–25 m). The boundary between segments 1 and 2 was put at $y = 72$ km (Fig. 1 ⊙) and r was taken to be constant for simplicity. The offshore distance of integration was about twice the slope width in each segment (60 and 15 km for segments 1 and 2, respectively). We computed the first four CTW modes in both segments using a grid of 50 vertical by 100 horizontal points. This rather high resolution was necessary to determine the first four modes well in segment 2 (see below).

The product δ_{mn} of the normalized CTW modes should ideally be zero for $m \neq n$ (1 for $m = n$). We calculated δ_{mn} to check if our Gotland CTW modes are well determined. For segment 1, $\delta_{mn} < 0.01$ ($m \neq n$) for all combinations of the first four modes. For segment 2, δ_{mn} increased from 0.02 for $m, n = 1, 2$ to 0.12 for $m, n = 3, 4$. The rather extreme topography/stratification combination of segment 2 apparently stretches to the limit this numerical method for mode determination (see also Brink and Chapman 1987). Poor orthonormality results were obtained for stronger stratification or steeper topography than we used in segment 2, even for increased spatial resolution in the numerical calculations.

CTW mode 1 in segment 1 has a highly barotropic structure, as expected, and a phase speed of 1.03 m s^{-1} (Fig. 5 ⊙, Table 2 ⊙). As is usual for CTWs, this phase speed is greater than for the continental shelf wave (0.78 m s^{-1}; e.g., Huthnance 1978). Mode 2 is more influenced by stratification, has a bottom-trapped maximum near 60-m depth and propagates northward at only 0.37 m s^{-1} (Fig. 5 ⊙, Table 2 ⊙). In segment 2, both modes are highly baroclinic, as expected. Mode 1 has a two layer, Kelvin-wave-like structure with a nodal line at about 60-m depth at the top of the halocline and a phase speed of 0.68 m s^{-1}. Mode 2 has a three-layer structure with a maximum near 50 m, nodal lines intersecting the bottom near depths 25 and 75 m, and a phase speed of 0.33 m s^{-1}. At first glance, EOF modes V1 and V2 resemble CTW modes 1 and 2 of segment 2. Higher CTW modes (not shown) have more vertical structure and are trapped closer to the coastal/bottom boundary. Phase speeds of modes 2 through 4 are slightly higher in segment 1 than in segment 2 (Table 2 ⊙). Lower modes are forced more efficiently by the wind although this is less pronounced for segment 2 (b_n in Table 2 ⊙). Frictional decay affects higher modes much more than lower modes, and this decay tends to be stronger in segment 1 than in segment 2 (a_{nn} in Table 2 ⊙). For example, alongshore decay scales (proportional to a^{-1}_{nn}) for mode 1 are longer by at least a factor of 10 than for mode 4. Likewise, frictional coupling is strongest between the higher modes (a_{nm}, $m \neq n$, not shown).

Our RCM observations extended into late fall 1977 but, unfortunately, hydrographic profiles from the west coast of Gotland are only available from the August intensive study period. To estimate the effect of seasonally changing stratification on our results, we recalculated the CTW modes using a "winter" stratification (permanent halocline but no thermocline; Fig. 5e ⊙, dashed line). For this case, mode structure in segment 1 became somewhat more bottom trapped (since the deep halocline now dominates the stratification) and the phase speeds decreased slightly (Table 2 ⊙). In segment 2, the nodal lines deepened for all modes and phase speeds decreased by 10%–20% (Table 2 ⊙). The lower phase speeds are due to slower internal wave phase speed in winter. In segment 2 in winter, wind forcing is distributed a bit more evenly between modes and frictional decay is somewhat stronger for higher modes (Table 2 ⊙). In all calculations below we use our observed, intensive study period (summer) stratification unless stated otherwise.

Calculations for the scattering of CTW modes among the first four modes at the segment 1–segment 2 boundary yield q_{nn} = 0.982, 0.964, 0.972, and 0.953 for modes 1, 2, 3, and 4, respectively. This indicates that only 3.6%, 7.2%, 5.5%, and 9.2% of the energy entering the boundary in modes 1, 2, 3, and 4, respectively, is scattered among other modes there. Almost all the energy lost by mode 1 in this process is recovered in mode 2 (q_{nm} for $n \neq m$, not shown). The above scattering formulation satisfies energy conservation for an infinite number of modes. Since we use only the first four modes here, total energy leaving segment 1 will be less than that passed to segment 2. In practice such a truncation error may not be important since most CTW energy is usually concentrated in the lowest modes. Our results below show this to be the case off Gotland. For the winter stratification, we find more scattering of CTW energy (q_{nn} = 0.948, 0.868, 0.883, and 0.934 for modes 1, 2, 3, and 4, respectively).

To calculate the ϕ_n, given the above results, we followed Clarke and Van Gorder (1986). Steps in alongshore distance and time used in the integration were 1 km and 6 h. Shorter steps in distance and in time did not change the results. The southern tip of Gotland (Hoburg) was chosen as the starting point of integration ($y = 0$) and the amplitude here was taken to be zero. This assumes that no significant amount of topographic wave energy arrives at Hoburg from Gotland's east coast or from the Swedish mainland. This crucial assumption is motivated by the shallow ridge (~ 20 m deep) extending far south from the island and the relatively deep ridge connection with the mainland to the south (~ 50 m deep in the shallowest part, Fig. 1 ⊙). For comparison with our observations, model runs were initiated on 3 August and completed on 28 November. The model was driven by alongshore wind stress from Hoburg ($y = 0–31$ km), Stora Karlsö ($y = 32–72$ km), and Visby ($y = 73–103$ km, the study area).

c. Comparison with recording current meter data

We performed a large number of simulations with various versions of the CTW model described above and compared simulation outputs at the positions of our two RCMs with LP alongshore current observations. A selection of these comparisons is presented in Table 3 ⊙. We used correlation and regression coefficients as a simple, quantitative measure of the simulation fit to observed data (e.g., Mitchum and Clarke 1986; Chapman 1987). Some of the changes in the correlation and regression coefficient in Table 3 ⊙ are statistically significant only at a rather low confidence level. In general, simulations and observations are well correlated and small variations in the parameters of the linear regression reflect small changes in the fit.

A rather good fit to data was achieved with the simplest model of CTW mode 1 only and no bottom friction and scattering. In this case, however, fluctuation amplitudes were underestimated at 70 m, overestimated at 90 m, and model simulations led data at 90 m. When this simplest model was expanded to also include mode 2, the correlation with data decreased slightly at 70 m, increased significantly at 90 m, and model amplitudes and phases at both positions were brought into good agreement with the data. Finally, when mode 3 and then modes 3 and 4 are also included in the frictionless case without scattering, the model fit to data only improves slightly at 70 m but degrades somewhat at 90 m (Table 3 ⊙). Simulations were then considered that include bottom friction but not scattering. Higher CTW modes are more strongly damped by bottom friction than lower modes (Table 2 ⊙) but, on the other hand, receive energy from lower modes through frictional coupling. For the case of modes 1–4, these processes lead to a slightly better fit to data at both depths for small bottom friction ($r = 0.005$ cm s^{-1}) than for the frictionless case (Table 3 ⊙). Larger bottom friction ($r = 0.02$ cm s^{-1}) apparently leads to too much damping and frictional coupling, degrading model fit to data at 90 m and, in particular, at 70 m.

Complete model simulations including bottom friction and scattering do not lead to significant improvements in fit to data compared to simulations with bottom friction only (Table 3 ⊙). For winter stratification, the q_{nm} reported above indicate that scattering is more important. For this case, the fit to data at 70 m improves considerably when scattering is included. Since the winter stratification used here differs from the summer stratification in the upper part of the water column only, changes in mode structure and simulated currents are greater at 70 m than at 90 m. For forcing by Hoburg winds only, the fit to data improves somewhat and model amplitudes decrease slightly for all model versions considered. This is consistent with results of the above correlation analysis between observed winds and RCM currents.

The above results and Ockham's Razor lead us to choose the CTW model with modes 1 and 2 only (summer stratification), no friction nor scattering, and Hoburg winds only as our preferred model for low-frequency current fluctuations near the west coast of Gotland during late summer and fall 1977. Figure 6 shows a comparison between low-passed alongshore flow observed at 70 and 90 m and the simulated alongshore flow at these positions for this model. Model fit to data at both depths is quite good during the first month or so (including the intensive study period). Later on, the fit at 90 m remains very good, while the fit at 70 m degrades considerably. In this latter period (when data on stratification was lacking), the phase of the model fluctuations at 70 m agrees well with those of the observations but the amplitudes are significantly underpredicted, particularly during strong events. The simple CTW model above holds for small amplitude fluctuations. During large amplitude events, CTW modal structure will be "swept" up and down past fixed positions. The 70-m depth is near the nodal depths of the lower CTW modes and thus will be more sensitive to such effects than the 90-m depth. In light of these and other possible complications, it is notable that the very simple model used here is able to hindcast observed currents off Gotland as well as shown here.

d. Comparison with pendulum current meter data

Figure 7 shows the wind stress at Hoburg, Stora Karlsö, and Visby; time–depth plots of observed PCM alongshore flow at station 3; and time–depth plots of simulated alongshore flow there from our simple CTW model. In general, below about 30-m depth, the model reproduces reasonably well the structure and amplitudes of the observed low-frequency fluctuations at station 3 during the intensive period. One prominent feature in the PCM observations is the apparent upward displacement of a maximum of southward flow. This maximum appears at the bottom on 25 August and can be followed up to 40-m depth on 27 August. This upward displacement is also captured well by the model although model simulations lag observations somewhat. In our simple, frictionless model with only the first two CTW modes, this feature is due to the arrival of the wind-driven current fluctuations associated with mode 2 after those associated with mode 1. If we assume zero CTW wave amplitude at the southern tip of Gotland (the reasonable fit of our results to data support this), then amplitudes of both modes depend only on the local wind. Phase velocities of the modes (Table 2) and the mean distance over which they are forced (52 km) give a mean lag of 25 h of mode 2 after mode 1 in the study area. This lag is consistent with the observed structure in Fig. 7 and with the observed lag of low-frequency RCM currents at 70 m after those at 90 m (Fig. 3c).

In contrast, the simple CTW model is not able to simulate the phase and amplitude of the observed alongshore currents in the upper 30 m at station 3 during the intensive period (Fig. 7). For example, a maximum in northward flow was observed in the surface layer on 24 and 25 August, before the maximum in northward wind stress on 26 August, while the model yields a flow maximum after the wind stress maximum. Still, PCM observations of the alongshore flow in the surface layer also reflect the synoptic-scale fluctuation (these currents are captured to a large extent by EOF mode 1). Simulations with the more complex model versions (not shown) did not improve on this situation. Other processes act on the surface layer such as direct wind-forcing (i.e., cross-shore component of the wind stress, which can drive an alongshore Ekman transport) or mesoscale eddies. Also, we cannot rule out a contribution to the PCM observations from inertial oscillations in the surface layer. A better fit to the data in the lower, rather than in the upper, part of the water column has been a common feature of applications of CTW models to shelf and slope circulation (cf. Chapman 1987).

6. Discussion

Here daily profiles of density and current velocity taken during 10 days along a short section off the northwest coast of the island of Gotland during the late summer of 1977 are analyzed together with recording current meter data from late summer and fall of that year at 70 and 90 m at a water depth of 100 m and at 4 km from the coast on the same section. RCM current data at both depths were dominated by large, low-frequency fluctuations in alongshore flow. These fluctuations were anticorrelated with regional wind observations, whereby better correlations were found with winds from the southern tip of the island than with local winds. Coherence was high between current fluctuations at 70 and at 90 m, whereby flow at 90 m clearly led flow at 70 m. An EOF analysis of these observations showed that variability in current and vertical isopycnal displacement was dominated by a strong, 7-day period, baroclinic fluctuation "trapped" in the coastal zone. This fluctuation is also apparent in the RCM data and is concurrent with a wind event of similar period. The EOF current analysis revealed a two- and a three-layer structure associated with the fluctuation. The time series of the (weaker) three-layer mode was found to lag that of the (stronger) two-layer mode by about one day.

These results suggest that wind-forced, coastal trapped wave theory may be useful in interpreting observed low-frequency fluctuations off the west coast of Gotland. Here we applied this theory (including bottom friction and scattering) to that coast and compared model output with our study area data. In our application, we assumed zero CTW amplitude at the southern tip of the island, the starting point for our forced wave integration, and used two coastal segments (wide shelf off southwest Gotland, narrow shelf off northwest Gotland; Fig. 1), both with a mean buoyancy profile from our intensive period observations. We considered three segments for wind forcing along the coast using observations at Hoburg, Stora Karlsö, and Visby (Fig. 1).

Our main result is that a very simple CTW model (first two CTW modes only, no bottom friction nor scattering, and forced by Hoburg winds only) is able to reproduce quite well amplitudes and phases of observed alongshore current fluctuations in the lower part of the water column in the study area. In particular, model fit to RCM current data at 90 m is excellent. Model correlation with data is considerably greater than correlations between local wind stress and the data. Thus, the simple wind-driven CTW model demonstrates considerable skill in hindcasting deep current fluctuations observed off the west coast of Gotland.

On the other hand, the CTW model was not as successful in the upper-water column. Other applications of CTW models to shelf and slope circulation have had the same problem (cf. Chapman 1987). A different source of variability in the Baltic Sea is the large-scale response of the basin to variable atmospheric forcing. In the synoptic band, this response can be separated in a "large scale" barotropic interior part and in a coastal boundary layer with CTW-like dynamics (cf. Walin 1972a,b). While the complicated bottom topography in the Baltic Sea may distort this simple picture, 3D numerical models show this general behavior (Krauss and Brügge 1991). In the open Baltic Sea, wind forcing over variable bottom topography may cause eddy formation. CTD observations there reveal eddies with 20–50-km scales (Aitsam and Elken 1982). Basin-scale flow and/or eddies may help explain our upper-water column observations.

Both the RCM data and the profiling current data show upward phase propagation at mid and lower depths. Bottom friction may cause vertical and cross-shore phase differences in alongshore flow (Brink 1982), but our results imply that the observed phase propagation is probably due to the superposition of CTW modes: in the "narrow shelf" segment, CTW modes 1 and 2 have a two- and a three-layer structure, respectively. Mode 1 propagates much faster than mode 2 and wind-forced fluctuations associated with mode 2 will arrive after those fluctuations associated with mode 1, forced by the same wind. Upon arrival at the study site, mode 2 current fluctuations would tend to add to those from mode 1 at middepths and to subtract from those of mode 1 deeper down. Such lagged superposition then leads to the observed upward phase propagation.

Why does CTW model performance not improve significantly when more modes, bottom friction, scattering, and winds from more coastal sites are included? From the spectra of time series of calculated CTW amplitudes (Φ_n) in the study area (not shown), we found that, even without friction, modes 3 and 4 arriving there contained much less energy compared to modes 1 and 2 than would be expected from the wind coupling coefficients only (b_n, Table 2 ⊙▬). This can be explained as follows: From the phase speeds in Table 2 ⊙▬ and Gotland geometry, modes 1, 2, 3, and 4 take 1.3, 3.3, 5.8, and 8.0 days, respectively, to travel from the southern tip of the island to our study site. Synoptic-scale events of typically one-week period dominate local wind conditions (Fig. 2 ⊙▬). Thus modes 1 and 2 would typically experience winds of one direction during their journey to the study site while modes 3 and 4 would experience winds of opposing directions, tending to cancel out the amplitude of these modes by the time they reach the study site.

When bottom friction is included in the CTW model, higher modes are more strongly damped than lower modes but receive energy from lower modes through frictional coupling. An investigation of Φ_n spectra for the case of modes 1–4 and small friction ($r = 0.005$ cm s^{-1}) again show much less energy in modes 3 and 4, probably still a "geometric filter" effect (see above). For the case of modes 1–4 and larger friction ($r = 0.02$ cm s^{-1}), apparently too much damping and frictional coupling has occurred, degrading model fit to data, in particular at 70 m where amplitudes have decreased as energy is transferred to modes trapped closer to the coastal boundary. In contrast, such a "high" value for r has been used in other CTW applications (e.g., Clarke and Brink 1985; Chapman 1987). In a strongly stratified system like the Baltic Proper, however, buoyancy forces may inhibit the formation of a bottom Ekman layer, thereby reducing the effects of the bottom friction on low-frequency flow (MacCready and Rhines 1993). Perhaps the relative success we have had in applying the CTW model to such a shallow system has depended upon such suppression of bottom boundary effects.

Bottom topography changes are considerable along the west coast of Gotland (and strongly affect CTW mode structure and properties; Figs. 1 ⊙▬ and 5 ⊙▬, Table 2 ⊙▬). Still, our calculations indicate that these changes are not great enough to give significant scattering among the CTW modes in the strongly stratified, summer situation. For weaker, winter stratification, however, we calculated considerably more scattering among modes and at 70 m, such scattering was needed in the winter situation to achieve good fit to data. Our results imply that winds from Hoburg are representative for winds acting near the west coast of Gotland upstream from our study area. The use of more wind data along such a short stretch of coast is apparently not motivated, in particular when local effects may compromise wind data quality, as may be the case at Visby.

Strong stratification in the Baltic Proper acts to restrict vertical exchange. Large pycnocline displacements, enhanced current shear, and enhanced near-bottom currents associated with strong coastal-trapped waves that we observed off the west coast of Gotland should help promote vertical exchange in the nearshore zone. It is interesting to speculate on the fate of the coastal-trapped waves after they reach the northern tip of the island. A shallow ridge extending north of Gotland (Fig. 1 ⊙▬) might continue to guide their energy as topographic waves. Will part of the CTW energy make its way back south along the Gotland east coast (our good fit to data based on the condition of zero CTW amplitude at the southern tip of

Gotland implies that not much CTW energy makes its way from the east coast to the west coast)? Will some CTW energy be recovered as mesoscale eddies off the northern tip of the island?

REFERENCES

Aitsam, A., and J. Elken, 1982: Synoptic scale variability of hydrophysical fields in the Baltic proper on the basis of CTD measurements. *Hydrodynamics of Semi-enclosed Seas,* J. C. C. Nihoul, Ed., Elsevier, 433–468..

Akima, H., 1970: A new method of interpolation and smooth curve fitting based on local procedures. *J. Assn. Comput. Mach.,* **17,** 589–602..

Brink, K. H., 1982: The effect of bottom friction on low-frequency coastal trapped waves. *J. Phys. Oceanogr.,* **12,** 127–133..

—— ,1989: Energy conservation in coastal-trapped wave calculations. *J. Phys. Oceanogr.,* **19,** 1011–1016..

—— ,1991: Coastal-trapped waves and wind-driven currents over the continental shelf. *Annu. Rev. Fluid Mech.,* **23,** 389–412..

—— ,and D. C. Chapman, 1987: Program for computing properties of coastal-trapped waves and wind-driven motions over the continental shelf and slope. Woods Hole Oceanographic Institution. Tech. Rep. WHOI-87-24, 122 pp. [Available from Woods Hole Oceanographic Institution, Woods Hole, MA 02543.].

Cederlöf, U., J. Rodhe, L. Rydberg, and P. Sehlstedt, 1996: Performance study of the Haamer gelatin pendulum current meter. *J. Sea Res.,* **35,** 55–61..

Chapman, D. C., 1987: Application of wind-forced, long, coastal-trapped wave theory along the California coast. *J. Geophys. Res.,* **92,** 1798–1816..

Clarke, A. J., and K. H. Brink, 1985: The response of stratified, frictional flow of shelf and slope water to fluctuating large-scale low-frequency wind forcing. *J. Phys. Oceanogr.,* **15,** 439–453..

—— ,and S. Van Gorder, 1986: A method for estimating wind-driven frictional, time-dependent stratified shelf and slope water flow. *J. Phys. Oceanogr.,* **16,** 1013–1028..

Csanady, G. T., 1981: Circulation in the coastal ocean. *Eos, Trans. Amer. Geophys. Union,* **62,** 9–11, 41–43, 73–75..

Davis, R. E., 1976: Predictability of sea surface temperature and sea level pressure anomalies over the North Pacific Ocean. *J. Phys. Oceanogr.,* **6,** 249–266..

Denbo, D. W., and J. S. Allen, 1987: Large-scale response to atmospheric forcing of shelf currents and coastal sea level off the west coast of North America: May–July 1981 and 1982. *J. Geophys. Res.,* **92,** 1757–1782..

Gustafsson, T., and B. Kullenberg, 1933: Untersuchungen von Trägheitssttrömungen in der Ostsee. *Sven. Hydrogr.-Biol. Komm. Skr., Hydrogr.,* No. 13..

Haamer, J., 1974: Current measurement with gelatin pendulums. *Vatten,* **1,** 49–52..

Huthnance, J. M., 1978: On coastal trapped waves: Analysis and numerical calculation by inverse iteration. *J. Phys. Oceanogr.,* **8,** 74–92..

Johnson, E. R., 1991: The scattering at low frequencies of coastally trapped waves. *J. Phys. Oceanogr.,* **21,** 913–932..

Krauss, W., and B. Brügge, 1991: Wind-produced water exchange between the deep basins of the Baltic Sea. *J. Phys. Oceanogr.,* **21,** 373–384..

Lass, H. U., and L. Talpsepp, 1993: Observations of coastal jets in the Southern Baltic. *Cont. Shelf Res.,* **13,** 189–203..

MacCready, P., and P. B. Rhines, 1993: Slippery bottom boundary layers on a slope. *J. Phys. Oceanogr., 23,* 5–22..

Mitchum, G. T., and A. J. Clarke, 1986: The frictional nearshore response to forcing by synoptic scale winds. *J. Phys. Oceanogr., 16,* 934–946..

Shaffer, G., 1979: Conservation calculations in natural coordinates (with an example from the Baltic). *J. Phys. Oceanogr., 9,* 847–855..

Walin, G., 1972a: On the transient response to meteorological disturbances in the Baltic. *Tellus, 24,* 1–18..

—— ,1972b: Some observations of temperature fluctuations in the coastal region of the Baltic. *Tellus, 24,* 187–198..

Tables

Table 1. Means and variances of low-passed, current component records and eddy kinetic energies ($K_e = (1/2)(u'^2 + v'^2)$) observed at the mooring station at 70 m and 90 m in a water depth of 100 m (Fig. 1). The half-power point of the low-pass filter was 40 h. Positive u and v are toward 113° and 23°, respectively, $|V|_{max}$ is the maximum speed observed in the raw records.

Click on thumbnail for full-sized image.

Table 2. Values of phase speeds (c_n), wind forcing coefficients (b_n), and frictional coefficients (a_{nn}) for the first four CTW modes off the west coast of Gotland. The values were calculated for a mean topography of each coastal segment (Fig. 1) and for summer and winter stratification (Fig. 6). The a_{nn} were calculated for a bottom friction coefficient of 0.005 cm s^{-1}.

Click on thumbnail for full-sized image.

Table 3. Selected results of the regression of CTW model simulations against demeaned and detrended, low-passed, alongshore current measured at a depth of 70 and 90 m off the west coast of Gotland. Simulations use different numbers of modes, different bottom friction coefficients (r, in cm s^{-1}), scattering due to changes in bottom topography or no scattering and winds from three coastal sites, or Hoburg (Fig. 1) winds only applied to the entire coastal stretch. Calculations have about 30 degrees of freedom estimated from an integral timescale (Davis 1976). Regression coefficients greater than 1 indicate model amplitude less than observed; positive lag indicates model output lagging observations.
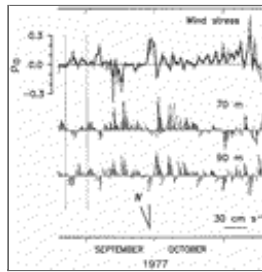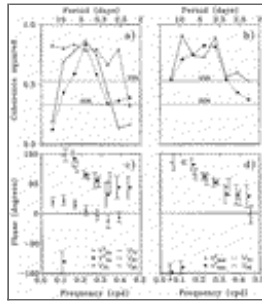

Click on thumbnail for full-sized image.

Figures

Click on thumbnail for full-sized image.

Fig. 1. The Baltic Sea and the study area off the west coast of the island of Gotland. Shown are the locations of repeated CTD and pendulum current meter profiles (dots), moored current meter observations (circle), and wind observations (triangles), as well as the two coastal topography segments used in the forced coastal trapped wave calculations (depths are in meters).
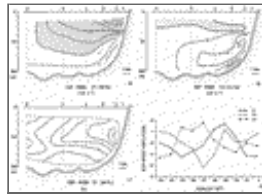
Click on thumbnail for full-sized image.

Fig. 2. Low-passed time series of alongshore wind stress at Hoburg (dashed line, positive toward 0°), Stora Karlsö (thin line, positive toward 0°), and Visby (thick line, positive toward 23°) as well as low-passed time series of alongshore flow at 70 m and 90 m in a water depth of 100 m, 4 km from the coast in the study area (upward toward 23°). See Fig. 1 ⊙= for locations. The vertical dashed lines mark the start and end of the intensive period study.
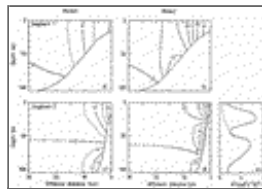

Click on thumbnail for full-sized image.

Fig. 3. Coherence (a) and phase (c) between low-passed, alongshore wind stress at Visby and low-passed, alongshore current at 70 m (crosses) and 90 m (dots) in the study area as well as coherence (b) and phase (d) as above but with Hoburg winds. Also shown are the coherence (a) and phase (c) between low-passed, alongshore current at 70 and 90 m (triangles). The bars in the phase spectra indicate the 95% confidence interval. Only phase results for coherence squared values above the 80% confidence level are plotted.

Click on thumbnail for full-sized image.

Fig. 4. Spatial structure of EOF modes 1 (a) and 2 (b) of alongshore velocity, and EOF mode 1 (c) of isopycnal depth, based on CTD and pendulum current meter observations from 10 consecutive days (23 August–1 September 1977) in the study area (Fig. 1 ⊙=). Dots show the mean depths of the individual observations. The dashed line in (c) outlines the domain within which mean depths to isopycnal surfaces can be calculated over the whole period. Also shown are the time series associated with these three modes (d).
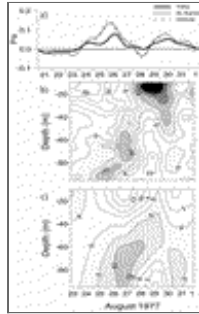

Click on thumbnail for full-sized image.

Fig. 5. Calculated alongshore velocity structure, using the summer stratification, for CTW mode 1 in coastal segment 1 (a), CTW mode 2 in segment 1 (b), CTW mode 1 in segment 2 (c), and CTW mode 2 in segment 2 (d), in arbitrary units. Also, shown in (e) is the summer (solid line) profile of squared buoyancy frequency (N^2, solid line), based on the intensive period data, and a N^2 profile chosen to be representative for winter conditions (dashed line).

Fig. 6. Demeaned and detrended, low-passed, alongshore flow (light lines) measured at 70 m (a) and 90 m (b) depth in the study area compared with CTW model simulations (heavy lines) of this flow. Simulations are for the first two CTW modes only, no bottom friction nor scattering, and Hoburg winds only.

Fig. 7. Alongshore wind stress at Hoburg, Stora Karlsö, and Visby during the intensive study period (a), space–time plot of alongshore velocity observed with the pendulum current meters at station 3 during this period (b), and space–time plot of simulated alongshore flow for this location and period with the simple CTW model with the first two CTW modes only, no bottom friction nor scattering, and Hoburg winds only (c).

Corresponding author address: Oscar Pizarro, Department of Oceanography, Earth Sciences Centre, University of Göteborg, Guldhedsg. 5, 413 81 Göteborg, Sweden.

E-mail: ospi@oce.gu.se